An Automobile Platform for the Measurement of Foehn and Gap Flows

GEORG J. MAYR, JOHANNES VERGEINER, AND ALEXANDER GOHM

Department of Meteorology and Geophysics, University Innsbruck, Innsbruck, Austria

(Manuscript received 27 August 2001, in final form 18 April 2002)

ABSTRACT

An instrument package to measure temperature, pressure, humidity, and position was designed to be quickly deployable on any automobile to be used for the study of gap and other orographically influenced flows. Differential GPS (global positioning system) measurements together with a distance counter gave the submeter accuracy of vertical position that was needed for observation of changes in the horizontal pressure field, which is an integral measure of the flow field aloft. A slantwise pressure reduction method was tailored for this application and verified with data from radio soundings. The automobile platform was successfully used during the field phase of the Mesoscale Alpine Programme (MAP) to classify flow states and observe hydraulic jumps in gap flows and to extend aircraft measurements to the ground.

1. Introduction

Point measurements continue to be the observational method of choice near the surface, whereas line (radiosondes, aircraft) or volume (remote sensing) measurements prevail in the atmosphere and for the earth's surface. The spatial density of the traditional surface network cannot keep up with the decrease in scale of the phenomena of interest both for operational and experimental use. The cost of operating such a network is too high for current budgets of weather services. The void is (partly) filled by public and private institutions that have started to operate their own meteorological networks in limited areas and mostly with a very narrow application in mind. The combination of all the networks might give sufficient spatial resolution even for meso-γ (Orlanski 1975) applications but poses several challenges: data exchange, quality standards, and intercomparability. Two successful examples are the operational MesoWest network in the western United States (Horel et al. 2000), and the network for the field phase of the Mesoscale Alpine Programme (MAP; Bougeault et al. 2001).

If the resolution is still too coarse, a mobile mesonet can be the solution. For example, a fleet of (originally 15) automobiles (Straka et al. 1996) instrumented with a pressure sensor with static head, temperature, relative humidity, wind, and position sensors has been used in the United States for the observation of near-surface airmass and wind field characteristics and the passage of gust fronts and mesocyclones. During a measurement campaign cars would be used partly in a stationary and partly in a roving manner.

The use of a automobile for the study of downslope windstorms had been pioneered during the Alpine Experiment in 1982. The automobile was used to get the researchers to predefined locations where measurements were taken and recorded manually. During the next large Alpine meteorological campaign, MAP (Bougeault et al. 2001), this idea could be taken further due to the advances in measurement technology. A subproject in MAP, ''dynamics of gap flow'' (GAP) was designed to study the influence of vertical and lateral contractions on the flow, and the coupling of the flow through the gap with the flow aloft (Mayr et al. 2002, manuscript submitted to *Meteor. Atmos. Phys.*, hereafter MAAB). Spatially and temporally dense observations of the mass and wind field were to be gathered for process studies and also the verification of numerical models. An automobile platform was designed to yield spatially dense (20–30 m) measurements of the mass field across the gap, and to extend the measurements from research aircraft to the ground.

Appropriate conservative variables for the distinction of air that originated at different altitudes are (virtual) potential temperature and mixing ratio, which require measurements of temperature, pressure, and humidity. Compared to the mobile Oklahoma mesonet, distances are much shorter and the terrain is not flat but consists of a deep valley with sloping terrain.

Since gap flow is shallow, hydraulic theory is a good, yet simple approximation to the full governing equations as it explains the salient features of the nonlinear gap flows (Armi and Williams 1983; Farmer and Armi 1999; Pan and Smith 1999; cf. section 4). Gaps can control

Corresponding author address: Georg Mayr, Institut für Meteorologie und Geophysik, Innrain 52, A-6020 Innsbruck, Austria.
E-mail: georg.mayr@uibk.ac.at

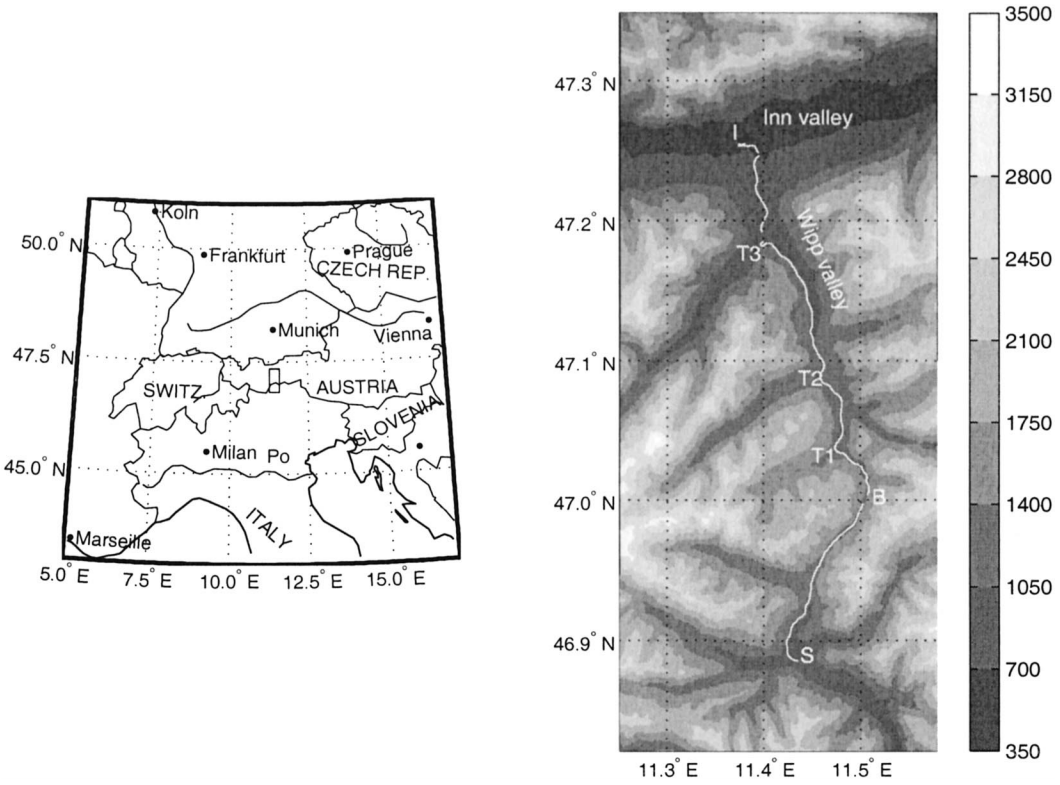

FIG. 1. Location of the MAP target area (rectangle) for the subproject dynamics of gap flow. The detailed map shows the course of the autobahn along which automobile measurements were taken in the Wipp Valley between Innsbruck (I) and Sterzing (S). T1, T2, and T3 are the first, second, and third western tributary valleys, respectively, north of Brenner (B). Elevation shading interval is 350 m MSL.

the characteristics of the flow and induce transitions from a deep, relatively slowly moving subcritical layer to a thin and fast moving supercritical (with respect to gravity wave speeds) layer. The flow returns into a subcritical state through a hydraulic jump—a turbulent transition to a deeper layer. Surface pressure is related to the potential energy of hydraulic flow. Knowledge of the pressure field, especially of its horizontal changes, allows deductions about the kinetic energy (wind) field aloft via Bernoulli's law, which states that (for incompressible, nonconducting, frictionless flow) the quantity

$$H = \frac{p}{\rho} + \frac{1}{2}|\mathbf{u}|^2 + gz \qquad (1)$$

is conserved along a streamline, where g is the acceleration of gravity, z is the height, p is pressure, ρ is density, $|\mathbf{u}|$ is a vector denoting speed,

Since pressure is measured along a sloping terrain, the exact height of the measurement location must be known and an appropriate reduction method applied before horizontal changes can be examined (cf. section 3).

The MAP target area for the dynamics of gap flows subproject composed the transect across the lowest pass through the alpine crest known as the Brenner (Fig. 1). Brenner Pass is a vertically stacked double pass (MAAB): the lower gap (~1400 m MSL) has only about 8% of the cross-sectional area of the upper one (~2100 m MSL). The field phase from 7 September through 15 November 1999 focused on southerly gap flow events, so that the upstream side was south of Brenner. One of the main alpine north–south traffic arteries runs from Innsbruck (580 m MSL; Austria) across Brenner (1370 m MSL) toward the Po Valley (Italy). It allowed passage through the region of interest in less than 45 min with slopes less than 7%. The spatially highly resolved ''snapshots'' from the automobile measurements were embedded in a larger spatial and temporal scale with the existing operational stations and the dedicated fixed research mesonet.

The next section of the paper describes the instrumentation, its calibration, and limitations, and the data storage and visualization in detail. A new method for pressure reduction tailored to the use with automobile-based measurements in sloping terrain is presented in section 3. A case study in section 4 showcases the capabilities of the instrumented automobile for gap flow.

2. Instrumentation

The scientific objectives of the instrumented vehicle were to define airmass characteristics and document horizontal pressure changes. This required temperature, hu-

FIG. 2. Components of automobile platform: case (which contains the battery and is used for storage and transport of the sensors), pressure sensor, temperature/humidity sensor, radiation shield, and laptop computer. The pressure sensor is placed in the middle of the back seat. The laptop stays in the passenger seat. The GPS unit (sensor and antenna integrated into the shape of a PC mouse) attaches to the roof with a magnetic foot. The radiation shield was mounted on a common roof rack and naturally ventilated during a measurement drive. The inset shows a near-frontal close-up of the radiation shield, which consists of two concentrical cylinders and two half-moon-shaped water shields, which are 40 mm apart. (The dimensions are in mm.) (b) Sideview of the radiation shield with airflow through it. (Lengths in mm.)

midity, pressure, and position measurements. The design is modular so that individual components can easily be exchanged or upgraded without having to revamp the whole setup. Data were logged to a laptop computer. This allowed the use of mainstream powerful measurement software instead of the more limited and often arcane software found in dedicated meteorological dataloggers. Another big advantage was the ability to visualize conserved flow variables in real time.

A limited budget forced the instrumental setup to be inexpensive and to be deployed on private vehicles. Therefore, another design goal was the quick (15 min) and easy installation in and on the automobile. Figure 2 shows the deployed platform. The carrying case also

TABLE 1. Specifications of meteorological sensors used in the automobile platform.

	Pressure	Temperature	Relative humidity
Model	Vaisala PTB 100A	Vaisala HMP233	Vaisala HMP233
Measurement range	800–1060 hPa	−40° to +60°C	0%–100%
Total accuracy (root sum of squares)	±0.3 hPa @ 20°C	±0.1 @ 0°C ± 0.005°C °C^{-1}	±2% (<90%) ±3% (>90%)
Response time (90%)	0.3 s	60 s (still air) ≈ 20 s @ 20 m s^{-1}	15 s (still air @ 20°C)

houses data logger, laptop computer, and battery during the measurements. The pressure sensor goes to the middle of the rear seat. The GPS sensor attaches to the roof. The pressure and humidity sensor are protected from radiation and adverse environmental influences inside a shield that mounts on a common roof rack.

The following description applies to the configuration of the instrument platform as it was used during MAP special observing period (SOP).

a. Pressure

Computation of potential temperature θ is relatively insensitive to pressure inaccuracies. A difference of 1 hPa changes θ by only 0.1 K. The detection of hydraulic jumps from horizontal pressure profiles, on the other hand, is more exacting and may require an accuracy better than several tenths of a hectopascal. In a typical measurement application, roads with a grade up to 7% are traveled at about 20–30 m s^{-1}. Accordingly, the maximum expected hydrostatic pressure change per second is ±0.2 hPa. That is about half the magnitude of weaker hydraulic jumps (cf. section 4). Therefore, the temporal response of the pressure sensor needs to be faster than 1 s. The other option for resolving the jump, driving more slowly, is not practically feasible on the autobahn, and will increase the time to traverse the gap, that is, the period during which the flow should remain quasi-stationary. A capacitive sensor (Vaisala PTB100A) met the accuracy and response-time criteria (cf. Table 1). Compared to the five-hole Pitot probes commonly used on aircraft, this type of sensor has the advantage of being inexpensive and very quick to deploy in the cabin of any car. One does not need a dedicated measurement vehicle. The greatest source of inaccuracy for that type of pressure sensor is its temperature dependence. The cabin temperature typically varies less than 5 K. Its value is measured so that the small remaining temperature dependence can be eliminated using the calibration polynomials (cf. section 2h). Pressure in the cabin is measured in the flow field disturbed by the automobile—unlike the five-hole probes, which are carried on long booms. Pressure measurements must therefore be calibrated for each car model and over the whole speed range (cf. section 2h). A practical drawback is that one cannot open windows (turbulent fluctuations) or turn on the fan. For example, fully turning up the fan in the automobile used here changed pressure by 0.4 hPa. The openings in the cabin intended by the car's designers for forced air exchange are sufficient for the pressure to equalibrate with the outside within the measurement interval of 1 s. This was tested by measuring the pressure signal in the parked automobile, while trucks were driving by.

b. Temperature

A combined resistance temperature and a capacitive relative humidity sensor (Vaisala HMP233; Table 1) was used. This type of temperature sensor has good absolute accuracy but a relatively long response time. The time constant of the temperature sensor can be too long when it is necessary to pinpoint the location of an airmass transition to within tens of meters. Results can be improved, though, with a devolution of the temperature signal.

A shield consisting of two horizontally aligned concentric cylinders and vertical half-circle protectors in the inner cylinder was custom-made to protect the temperature sensor from water/snow and radiative heating from above and from the roof of the automobile (Fig. 2). The shield was mounted on a regular roof rack approximately 40 cm above the roof of the automobile. The vertical half-circle protectors kept water and snow away from the sensor and slowed the flow down to reduce the kinematic distortion of the temperature measurement. The kinetic energy of the air against which the sensor moves is converted to internal energy as it hits the sensor and is compressed nearly adiabatically. How efficient that process is in raising the measured air temperature had to be determined empirically; again over the whole speed range of the automobile (cf. section 2h). Measurements with a hot-wire anemometer at the location of the temperature sensor in the shield showed that air flows by at a speed of 0.103 the speed of the automobile. The correlation coefficient of the linear fit is 0.89. For typical car speeds, the automobile sensor is naturally aspirated with about 3 m s^{-1}. A fan that can be attached to one end of the cylinder never had to be used, since no measurements were made while the car was parked. The forced ventilation measurements with the hot-wire anemometer were made without the fan attached to the shield.

c. Humidity

The requirement to be inexpensive allowed only for a relatively slow (Table 1) polymer sorption sensor. Ini-

tial trials with a dewpoint mirror were soon abandoned because of its even longer time constant and problems of keeping the mirror clean, especially from the salt used to keep the roads free of snow and ice during the cold season. The half-circle water shields (Fig. 2, inset) protected not only the temperature sensor but also the relative humidity sensor.

d. Wind

For a number of reasons, direct wind measurements were not made. First, it was not clear whether sufficient accuracy of wind measurements could be reached on windy and sloped roads with an inexpensive, quickly deployable instrument package. Second, instrumented aircraft experience suggests that wind measurements are of best quality while the plane is flying straight. Similarly, the mobile Oklahoma mesonet only uses wind measurements when the car is not accelerating (Straka et al. 1996). Third, regions with and without gap flow (e.g., orographically blocked air upstream and cold pools downstream of the pass) can also be detected from potential temperature alone. For all these reasons the automobile platform did not include an anemometer; only more than 30 fixed mesonet stations gathered wind data.

e. Position

Since knowledge of the height of the pressure sensor to less than a meter was crucial to establish horizontal pressure differences, the roads traveled were surveyed with differential global positioning system (DGPS). For some parts of the roads, the surrounding mountains allow only 2–3 h day^{-1} for the minimum of five satellites to be seen by the GPS receiver for an overdetermined solution to the three-dimensional position (and time). Even then measurements were difficult due to multipath of the satellite signals and ''loss of lock.'' With multipath the satellite signal does not directly reach the GPS receiver but bounces off the steep terrain. When using only pseudorange information the multipath positioning error can be as large as 10 m. The chosen antenna type minimized multipath effects, and the DGPS software dealt with most of the remaining instances. The most accurate vertical positioning is not attained using the GPS pseudorange information but the carrier phase information (e.g., Strang and Borre 1997, chapters 14 and 15), which has the additional advantage of small (at most a quarter-wavelength, $\sim$5 cm) multipath contamination. Measurements of the carrier phase cannot give the number of complete wavelengths between satellite and receiver, but only the additional *fraction* of a wavelength. It takes typically at least 15–30 s of measurements before the number of complete wavelengths and thus the exact distance to the satellite can also be determined. Buildings, tunnels, bridges, and mountains can interrupt the GPS signals. For 15–30 s after this loss of lock, the more precise phase positioning will not be available and the height derived from pseudorange information might be too inaccurate for our purposes.

Since it was very unlikely to encounter proper satellite constellations for DGPS elevation determination during the meteorological measurements, a different strategy had to be used. The roads were presurveyed with differential GPS at 1 Hz at locations approximately 20 m horizontally apart during these short periods when at least five GPS satellites were visible. Data were postprocessed to achieve maximum accuracy. Elevation under bridges and overpasses was linearly interpolated but left undetermined in tunnels where meteorological measurements could not be used anyway. The automobile position upon passing landmarks like traffic signs, bridges, and emergency telephones along the road was also presurveyed with DGPS. These landmarks are 500–3000 m apart.

The three-dimensional position during a meteorological campaign was then computed by mapping distances between the presurveyed landmarks from a car-transmission-based sensor to the presurveyed DGPS data. A mouse-shaped GPS receiver that easily mounted on the roof of the automobile with a magnetic foot (Garmin 35) was the backup system for the distance counter.

f. Visual information

Gap flows in the Brenner cross section are almost always moist enough to be accompanied by clouds. Clouds can make plunges of the air and hydraulic jumps visible as well as the top of a potentially colder air mass that can lie in the Inn valley and the exit of the Wipp Valley. Photos were taken from the automobile along the whole traverse.

Since wind was not directly measured (cf. section 2d), broad qualitative estimates of wind speed were visually made from flags and wind socks along the traverse.

All this visual information provided invaluable details about the flow. When the mobile platform was first used, this information was lost if no copilot was available to write it down. Later, the visual observations made were spoken onto a tape recorder and manually transcribed afterward. Now dictation goes to a digital recorder via a headset; it is processed by a speech recognition software after the drive.

g. Data storage and visualization

Data from all sensors were processed by a National Instruments' DAQCARD-AI-16XE-50 PCMCIA card with a 16-bit A/D converter in a laptop computer. Whereas the computer was powered through the automobile's cigarette lighter, the logging card and all sensors relied on a separate battery to minimize interference from the automobile's electric circuits.

An application was written in National Instruments' graphical programming language Labview to store the

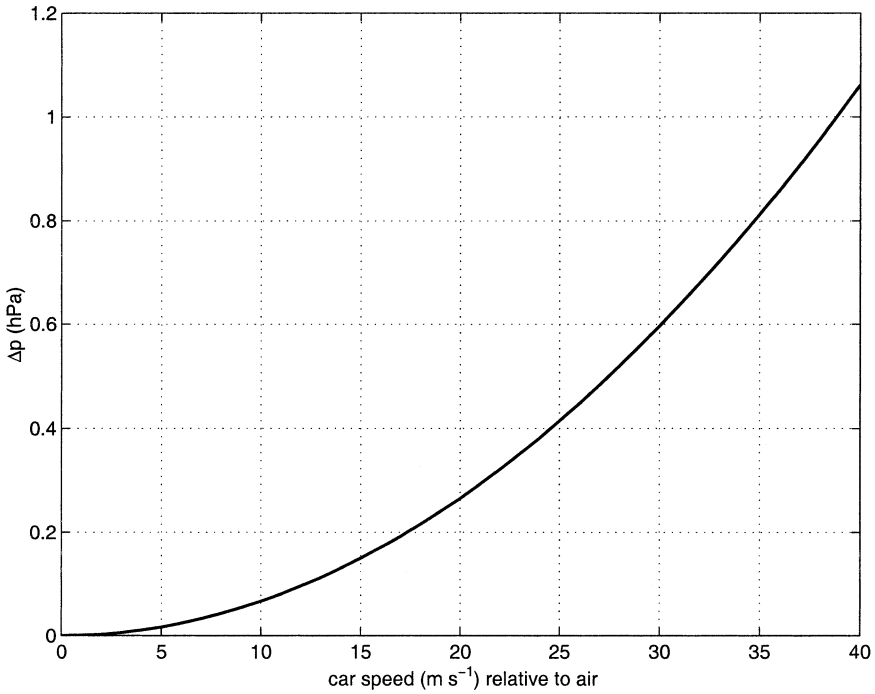

FIG. 3. Magnitude of dynamic pressure measured by the pressure sensor in the cabin of the automobile. The curve is a least squares fit to data from comparison measurements with a stationary pressure sensor. Typical car speeds (relative to ground) during gap flow measurements were 20–30 m s^{-1}; typical wind speeds 5–15 m s^{-1}.

data and visualize conserved variables in real time as a function of distance. Additionally, the numerical values from all sensors are displayed. This immediate visualization proved crucial in adapting the automobile route to conditions encountered and in relating visual information to measured variables.

h. Calibration

The temperature sensor was calibrated in a temperature-controlled (Haake DC5) water bath (Haake K20) against a traceable standard, a Testoterm Testo 781 quartz thermometer, between −10° and +30°C. The pressure sensor was calibrated against a Parascientific quartz barometer. The dynamics effects on temperature, pressure, and humidity measurements were experimentally determined on a long level stretch of a not-too-busy road from the difference measured while passing a reference station mounted at the side of the road. An overcast day was chosen to isolate the dynamic effects. Winds were less than 1 m s^{-1}. The automobile drove by the reference station in speed increments of roughly 3 m s^{-1} from 5 to 35 m s^{-1}. The resulting dynamic pressure difference reassuringly behaved according to Bernoulli's law (1) and related linearily to speed squared. The temperature difference also reads proportional to speed squared. The compressibility of air must be taken into account in this case by adding an internal energy term c_pT to Eq. (1), where c_p is the specific heat of air at constant pressure. Air molecules impinging on the sensor decelerate and their kinetic energy is converted to internal energy. The dynamical correction was 0.4 K at the fastest automobile speed. The dynamic effects on temperature and pressure were also taken into account for the computation of absolute humidity (e.g., mixing ratio) from the measured *relative* humidity.

i. Limitations of the mobile platform

1) DYNAMIC EFFECTS

Whereas the dynamic pressure effect through the movement of the automobile was corrected with Bernoulli's law (1) and the empirically determined efficiency constant, dynamic pressure from wind could not be accounted for with the instrumental setup used for MAP SOP. Wind was not measured for reasons stated in section 2d. A quad-plate static pressure port, as used in the mobile Oklahoma mesonet (Straka et al. 1996), was not considered at the conception of the instrumental package, since it would have required a tall structure on top of the automobile to keep the pressure port out of the automobile's boundary layer. With the added height, some roads with low overpasses could not have been traveled, and traffic laws forbid a hood boom similar to the nose booms used on research aircraft.

Figure 3 shows the magnitude of the modification to pressure resulting from movement of the automobile

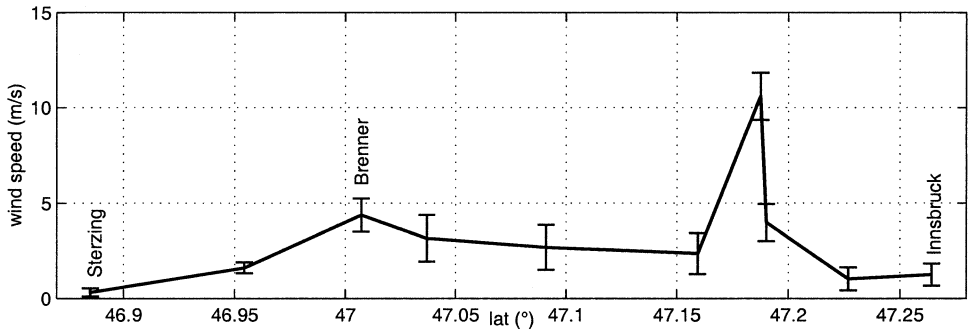

FIG. 4. Sustained wind speed of gap flow at fixed mesonet stations across Brenner Pass midmorning of 30 Oct 1999: mean and std dev (error bars).

relative to the *air*. Air-relative speed will be larger than ground-relative speed for headwind, and smaller for tailwind. Typical automobile speeds (relative to ground) were 20–30 m s^{-1}. Gap flow wind speeds as measured with the fixed mesonet varied smoothly with horizontal distance from the pass (Fig. 4). Therefore, the error resulting from only correcting for the dynamic effect of car speed but not wind speed was spread over a larger distance. Its magnitude was typically below 0.2 hPa, its sign depended on the direction of the wind relative to the heading of the automobile. There was only one short stretch of approximately 1.5 km where the rapid succession of low–high–low wind speeds made pressure measurements unusable for our purposes. For applications in different topographical settings where strong winds from the side can also occur, one could not get by without a static pressure port.

2) EXHAUST FROM OTHER VEHICLES

The autobahn across the Brenner is one of the busiest alpine north–south arteries. While car exhaust did not noticeably change temperature measurements, truck exhaust did when one had to drive immediately behind one or a whole convoy of them. Under normal conditions, trucks were quickly passed, though, since the speed limit for them is much lower than for cars. The resulting temperature spikes can easily be filtered; they are also mentioned in the voice record of the measurement campaign. An example can be found in the case study in section 4 (Fig. 5b). If passing was not possible (e.g., due to a slower passing car ahead or a construction zone), it was found that keeping more than 100-m distance and mounting the sensor on the driver's side of the automobile to increase the distance to the exhaust pipes of trucks being passed, made the effect unnoticeable in the temperature recording.

3. Pressure reduction

Pressure varies about a thousand times more in the vertical than in the horizontal. Horizontal pressure changes are telltale signs of gravity waves and hydraulic jumplike features in gap flows. Since the pressure measurements are along sloped terrain, the contribution of elevation change to the pressure signal has to be eliminated by hydrostatically ''reducing'' all measurements to a uniform height. However, the profile of the virtual temperature in the layer between the measurement height and the reduction height is usually unknown. This is a basic problem in meteorology and numerous schemes have been devised to obtain the ''best'' (in the sense of minimizing reduction artifacts) pressure field for the available data and given terrain (cf. Pauley 1998 and references therein).

A new algorithm was developed to exploit the particularities of the automobile data. The method is related to the ''horizontal reduction'' method (Mesinger and Treadon 1995) and the D-value scheme of Weaver and Toth (1990), which is based on concepts by Bellamy (1945) and Sangster (1987).

a. Slantwise reduction

The idea behind the reduction method used for the automobile measurements is simple. Since a dense profile of temperature, humidity, height, and pressure was measured along a slope on both sides of the gap, one does not need to rely on a fictitious atmosphere any more. The altitude–temperature relationship is *known* as long as the pressure reduction is *up*ward to the highest point of the measurements. This information still falls short of knowing the vertical temperature profile above each measurement point but is more valuable than having *one vertical* profile, for example, from a radiosonde: the temperature profile along a slope contains already a large part of the inevitable horizontal variations in the vertical temperature profile.

This *slantwise reduction* was performed using a cumulative summation of the hydrostatic pressure differences computed from virtual temperatures of all layers along the slope between the reduction level and a measurement point. There is a sublety, though. Air masses on both sides differed: the upstream side was colder (cf. Fig. 5a) and part of the air was blocked. Air from higher up descended adiabatically downstream of the gap, thus

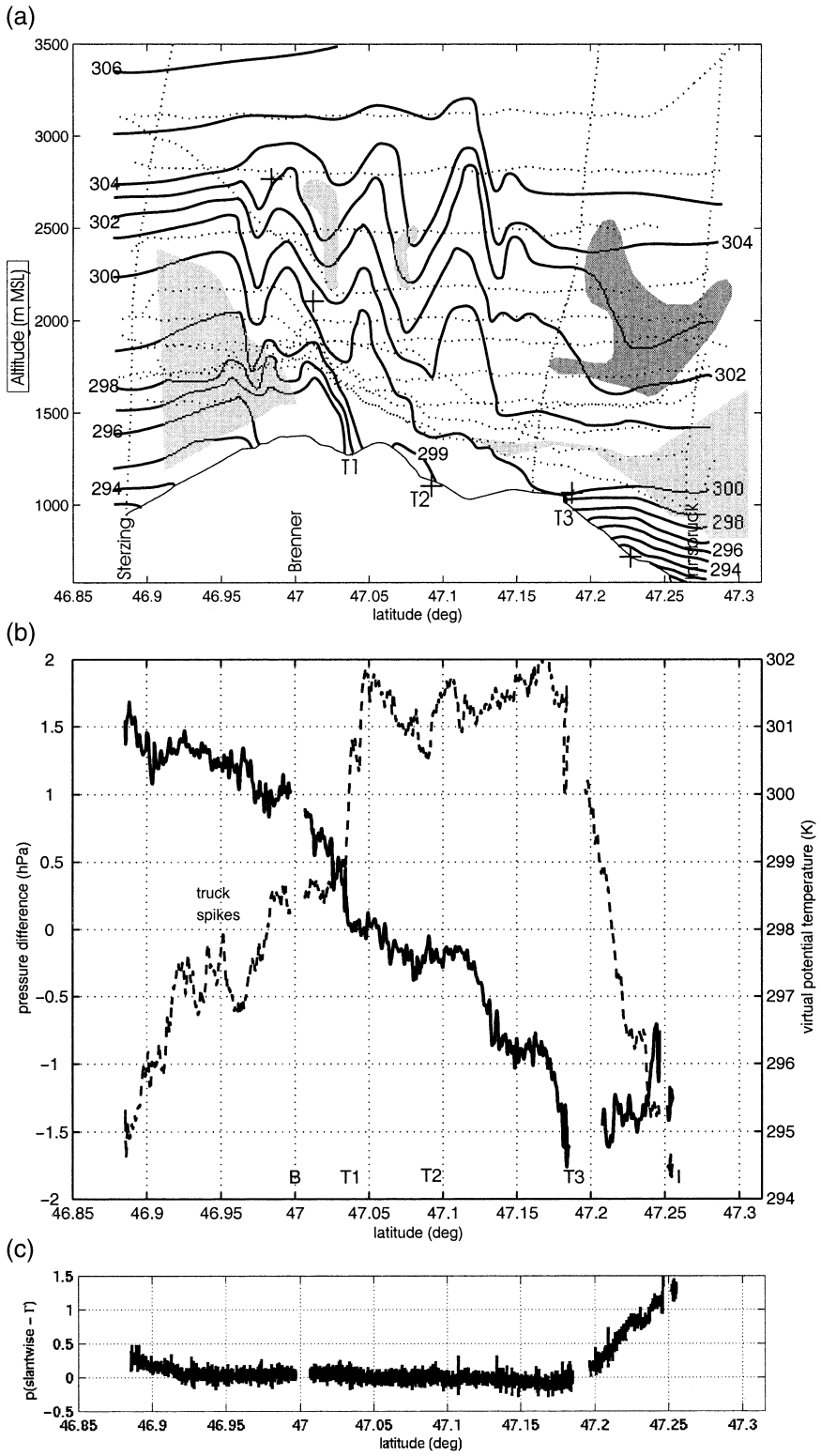

FIG. 5. Gap flow across Brenner Pass midmorning of 30 Oct 1999. (a) Vertical cross section of potential temperature (1-K isolines) and v component of wind (light shading for $v \leq 4$ m s^{-1}, dark shading for $v \geq 14$ m s^{-1}) from aircraft (dotted tracks), radiosondes (dotted), automobile (solid), and selected stations of the fixed mesonet (crosses). (b) Difference of reduced pressure (hPa) to pressure at downstream reduction level (solid), and virtual potential temperature (K; dashed). A spike in the potential temperature caused by having to drive to close to a convoy of

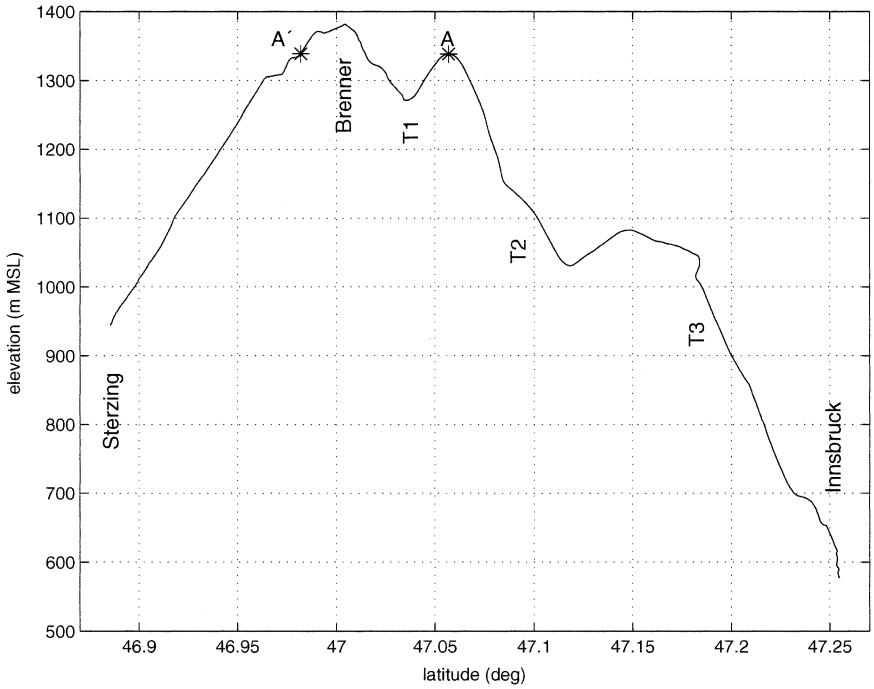

FIG. 6. Vertical profile of the automobile traverse across Brenner Pass along the autobahn. All pressure values between A′ and the downstream (northern) end were reduced to location A; values upstream of A′ were reduced to A′, which is at the same height as A. Locations of western tributary valleys are marked with T1, T2, and T3, respectively.

making the air there warmer. A slantwise reduction from both sides to the gap as the highest point in the profile will create an artificial discontinuity of the reduced pressure field at the gap, a place where there might be a hydraulic jump. This problem was circumvented by reducing pressure to the same height somewhat (approximately 50 m) below the gap on *both* sides of the gap. Pressure was then reduced with *three* slantwise temperature profiles: upstream (south) of A′ was reduced to A′ and all levels downstream of A′ were reduced to location A (Fig. 6). Part of the temperature profile for reduction of locations between A′ and the pass still consisted of the colder and more stable upstream air, so that the transition at A′ was continuous. For the Brenner transect depicted in Fig. 6, the reduction of all levels between A′ and A to A was actually beneficial. During gap flow events colder air reached across the pass to approximately A, before it was mixed with air that descended from the 700 m higher upper gap, whose cross-sectional area is approximately 13 times the one of the lower gap.

Isentropes in Fig. 5a show that a slantwise temperature profile captured most of the horizontal change of the vertical temperature profile between the surface and the reduction levels.

Figure 5c demonstrates how naively using temperature at the datum together with a constant temperature gradient (''one-point method'') fails when the vertical temperature structure consists of more than one layer. In the cold pools on both ends of the transect, the one-point method *under*stimated the layer-mean *temperature*, which made the associated hydrostatic pressure difference across the layer too high and thus the *reduced pressure* too *low*. The pressure difference across the pass, which is a simple one-number characteristic of the flow dynamics, was overestimated by about one-third!

b. Verification

Radio soundings launched a few kilometers away from the downstream endpoint of the automobile's traverse during the field phase of MAP allows one to compare slantwise reduction with vertical reduction and estimate the error from partly neglecting horizontal changes in the vertical temperature profile. This comparison was particularly exacting for two reasons. The com-

←

trucks (cf. section 2i) is marked. Data in tunnels are excluded as is reduced pressure at the location of the wind speed maximum. Geographical locations marked are Brenner (B), Innsbruck (I), and the first (T1), second (T2), and third (T3) western tributary valleys north of Brenner (cf. detailed map in Fig. 1). (c) Difference (hPa) between slantwise pressure reduction and one-point method with dry adiabatic lapse rate.

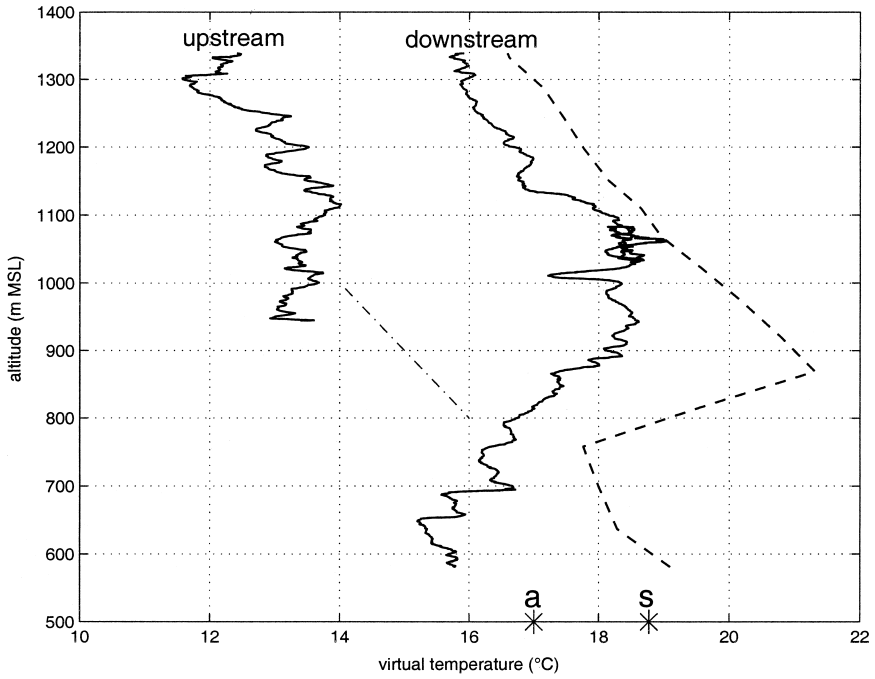

FIG. 7. Measurement drive 1000 UTC 30 Oct 1999: virtual temperature profiles below reduction level upstream and downstream of Brenner Pass together with the 1100 UTC radiosounding in Innsbruck (dashed). The site of the radiosonde launch is a few km away from the downstream end point of the drive. The latter is the reference location used for verification of various reduction methods with the Innsbruck sounding. The dashed–dotted line marks the dry adiabatic lapse rate. Stars on the abscissas indicate the layer mean temperature between the reference location and the reduction level from the automobile profile (a) and the sounding profile (s), respectively.

parison location is farthest—both vertically (~800 m) and horizontally (~30 km)—away from the reduction level. And often there was a 200–300-m-deep cold pool at the northern end of the drive.

The propagation of error for reduced pressure

$$p_r = p \exp\left[-\frac{g(h_r - h)}{R\overline{T}_v}\right] \tag{2}$$

is

$$\frac{\Delta p_r}{p_r} \cong \frac{g(h_r - h)}{R\overline{T}_v^2}\Delta\overline{T}_v - \frac{g}{R\overline{T}_v}\Delta(h_r - h) + \frac{1}{p}\Delta p. \tag{3}$$

The subscript r refers to the reduction level and h is height (m MSL). A change of reduced pressure by 1 hPa (with $\Delta h \sim 800$ m, $\overline{T}_v \sim 290$ K) can be caused by a difference in layer mean virtual temperature $\overline{T}_v$ of approximately 3.5 K, an uncertainty in height difference of 10 m, or in original pressure of 1 hPa.

Figure 7 compares slantwise reduction method for the 1000 UTC 30 October 1999 measurement drive with ''truth''—a vertical reduction using the 1100 UTC Innsbruck sounding. This case was chosen because of its nonuniform vertical temperature profile, for which simple traditional reduction schemes produce large errors. The virtual temperature profile of the sonde was warmer than the automobile profile used for the slantwise reduction. The 1.6-K difference for the layer-mean temperature gave a difference in reduced pressure of 0.4 hPa. The largest contribution to this difference came from different measurement times: the radiosonde in Innsbruck was launched at local noon, 70 min after the end of the measurement drive. Innsbruck had warmed 3 K during that period. This shows the advantage of reducing pressure with temperature and height from automobile measurements themselves instead of with values from the more infrequently launched radiosondes. Another contribution stemmed from the horizontal change of the vertical temperature profile with increasing distance from the gap (cf. Fig. 5a) that could not be completely captured by the slantwise temperature profile along the sloping ground. For example, air was adiabatically mixed above 870 m MSL in Innsbruck, but only above 1050 m MSL in the automobile profile.

Minor contributions to the difference could have come from the (short) spatial separation of sounding and automobile reference location, which are corrobated by preliminary high-resolution (800-m mesh) numerical simulations. The launch site is west of the exit region of the Wipp Valley.

In summary, the slantwise reduction method was within 0.1 hPa of the truth if the difference in measurement times is taken into consideration. Similar accuracies were found in other cases. Therefore, use of

the slantwise reduction method with careful selection of the reduction levels can keep reduction errors within the uncertainties of the radio sounding itself.

4. Application: Case study, 30 October 1999

The gap flow on 30 October 1999 was the best-observed flow of the whole MAP SOP. The synoptic background flow evolved unusually rapidly. The automobile traverse (to be discussed) was taken in the late morning from 1007 to 1042 UTC while the NOAA-P3 research airplane flew flight legs stacked every 300 m from approximately 300 m AGL up to 3500 m MSL (between 0930 and 1130 UTC). Only midlevel (As and Ac lent) and high-level clouds with a total coverage of six to seven octas were present; atypically, a foehn wall cloud on the upstream (southern) side was absent, which made low-level flights possible there.

The air in the basin upstream of Brenner Pass was cold, stably stratified, and blocked from flowing over the pass (Fig. 5b), which is at exactly 47°N. Pressure reduced with the slantwise method and plotted as difference to the pressure at the reduction level in Fig. 5b remained nearly constant on the upstream side. The transition from an increase of potential temperature with height to a nearly constant value [masked by spikes from truck exhaust, cf. section 2i(2)] north of 46.935°N, about 200 m below the pass, indicates where air first started to flow toward the pass. At the end of the steepest slope (cf. Fig. 6) north of the beginning of the narrowest part but well before the pass itself, pressure dropped abruptly by 0.4 hPa and stayed at the level to the pass itself. Potential temperature rose by almost 2 K from its previous level combined with the onset of 5 m s^{-1} winds as inferred from tree movement. Combining data from the NOAA-P3 aircraft, radio soundings, and the automobile (Fig. 5a) shows that isentropes plunged down at the location of the pressure drop and rebounded to a slightly higher elevation within a few kilometers. The rebound (''jump'') region had the lowest wind speeds. These features are the signature of a hydraulic jump. Hydraulic jumps commonly occur *down*stream of passes. The jump *up*stream of Brenner Pass had not been anticipated and surface stations had not been placed there to capture it. The variation across the plunge/jump region of the mean temperature of the layer between pass elevation and the upper edge of the plunging yielded a hydrostatic pressure change of 0.4 hPa—the same as the automobile-observed total pressure change.

As is shown in more detail in Armi and Mayr (2002, manuscript submitted to *Quart. J. Roy. Meteor. Soc.*), the Brenner Pass acted as a hydraulic control. Pressure upstream of the pass remained nearly constant (with the exception of the small upstream jump) as the flow was subcritical. With the transition to supercritical flow and the ensuing acceleration of the flow, pressure fell with increasing downstream distance from gap (Fig. 5b). The flow adjusted to the conditions farther downstream (a mountain range north of Innsbruck) in a hydraulic jump near the northern end of the automobile measurements, where pressure rose abruptly and wind speed aloft decreased by 10 m s^{-1}. Superimposed on these larger flow structures were several smaller-scale features. A few kilometers downstream of Brenner (marked with T1 in Fig. 1), potential temperature shot up more than 3 K and pressure dropped 0.5 hPa as air plunged from the upper gap to the ground. The aircraft measurements (Fig. 5a) confirmed these deductions from the automobile-based observations.

Other locations where air plunged from aloft could be deduced from the automobile measurements alone downstream of ridges, which protrude from the west into the Wipp Valley (locations T2 and T3), and downstream of a narrowing of the valley at 47.13°N. These deductions can be confirmed from the aircraft data with the exception of T3, over which the aircraft did not fly.

Air in Innsbruck in the Inn valley, at the northern end of the automobile measurements, was about 8 K (potentially) colder than the warmest air that had reached the floor of the Wipp Valley after its passage through the upper gap.

5. Conclusions

The previous section demonstrated that the automobile platform is an ideal tool for the ground-based observation of flows in mountainous terrain (as long as there are roads). Its spatially quasi-continuous measurements along the transect of a gap detected plunges and hydraulic jumps with a horizontal extent of only a few kilometers, which are hard to spot with a traditional, fixed mesonet, even one as dense as the one during MAP SOP with 35 stations observing pressure (MAAB). A mobile platform does not require a priori knowledge of where the phenomena of interest are. The hydraulic jump slightly upstream of Brenner Pass was not anticipated; accordingly no surface stations were sited there.

Setting up, maintaining, and dismantling the research mesonet for GAP took up a huge amount of manpower and time. At least as much effort had to be spent on preexperiment and postexperiment calibration and quality control of the data in order to be sure that features in the dataset reflected features of the flow and not of the sensors. The automobile platform was much quicker to deploy. It takes approximately 15 min to install the package in the automobile. Calibration took longer than for a fixed station since the speed dependence of the temperature and pressure readings had to be empirically determined. This calibration needs to be performed for each automobile type used. It will not be needed if a static pressure port can be used that has omnidirectional response and is unaffected by normally occurring tilt angles (relative to the wind vector) of less than 20° [e.g., the quad-disc static port (Nishiyama and Bedard 1991)].

Another application of the automobile platform is exploration, for example, for the siting of fixed mesonet

stations. How universal the findings from the gap flow experiment are, for example, will be explored with automobile-based measurements along gaps in the vicinity of the Wipp Valley.

An automobile platform can measure only individual cases. It gives information about the flow field near ground and—via pressure—about the integral characteristics of the flow aloft. Research aircraft ideally expand these measurements by providing detailed characteristics of the flow aloft. The temporal evolution of the flow field prior, during, and after such cases must be provided by a fixed mesonet, which also gives an estimate how typical or unusual an automobile/aircraft-observed case is.

Acknowledgments. Roland Mayr set up the data logging with some assistance from Franz Weitlaner and programmed the logging and visualization software. Rainer Diewald put the idea for the radiation shield into a tangible piece of equipment. Dr. Andreas Giez from flight facilities at DLR Oberpfaffenhofen is thanked for advice on the design of platform and calibration of the humidity sensor at their test stand. Special thanks to Prof. Larry Armi for insights to hydraulic flow behavior, discussions of the pressure measurements and of the 30 October case study, and for directing the NOAA P3 flights. We (and the manuscript) benefited greatly from the constructive comments and suggestions from two anonymous reviewers. Part of the funding for this research came from the Austrian Science Foundation (FWF-13489-TEC).

REFERENCES

Armi, L., and R. Williams, 1983: The hydraulics of a stratified fluid flowing through a contraction. *J. Fluid Mech.,* **251,** 355–375.

Bellamy, J. C., 1945: The use of pressure altitude and altimeter corrections in meteorology. *J. Meteor.,* **2,** 1–79.

Bougeault, P., and Coauthors, 2001: The MAP special observing period. *Bull. Amer. Meteor. Soc.,* **82,** 433–462.

Farmer, D., and L. Armi, 1999: Stratified flow over topography: The role of small-scale entrainment and mixing in flow establishment. *Proc. Roy. Soc. London,* **455A,** 3221–3258.

Horel, J., M. Splitt, and B. White, 2000: MesoWest: Cooperative mesonets in the western United States. Preprints, *Ninth Conf. on Mountain Meteorology,* Aspen, CO, Amer. Meteor. Soc., 265–268.

Mesinger, F., and R. E. Treadon, 1995: ''Horizontal'' reduction of pressure to sea level: Comparison against the NMC's Shuell method. *Mon. Wea. Rev.,* **123,** 59–68.

Nishiyama, R. T., and A. J. Bedard Jr., 1991: A ''quad-disc'' static pressure probe for measurement in adverse atmospheres: With a comparative review of static pressure probe designs. *Rev. Sci. Instrum.,* **62,** 2193–2204.

Orlanski, I., 1975: A rational subdivision of scales for atmospheric processes. *Bull. Amer. Meteor. Soc.,* **56,** 527–530.

Pan, F., and R. B. Smith, 1999: Gap winds and wakes: SAR observations and numerical simulations. *J. Atmos. Sci.,* **56,** 905–923.

Pauley, P. M., 1998: An example of the uncertainty in sea level pressure reduction. *Wea. Forecasting,* **13,** 833–850.

Sangster, W. E., 1987: An improved technique for computing the horizontal pressure-gradient force at the earth's surface. *Mon. Wea. Rev.,* **115,** 1358–1369.

Straka, J. M., E. N. Rasmussen, and S. E. Fredrickson, 1996: A mobile mesonet for finescale meteorological observations. *J. Atmos. Oceanic Technol.,* **13,** 921–936.

Strang, G., and K. Borre, 1997: *Linear Algebra, Geodesy, and GPS.* Wellesley-Cambridge Press, 624 pp.

Weaver, J. F., and J. J. Toth, 1990: The use of satellite imagery and surface pressure-gradient analysis modified for sloping terrain to analyze the mesoscale events preceeding the severe hailstorms of 2 August 1986. *Wea. Forecasting,* **5,** 279–298.